J Therm Anal Calorim (2010) 101:541–547
DOI 10.1007/s10973-010-0827-4

Investigation of the CuBr–LiBr phase diagram

Edward Krzyżak · Alina Wojakowska · Andrzej Wojakowski · Marek Wołcyrz

CCTA10 Special Issue

Abstract Phase diagram for the system CuBr–LiBr was determined by differential scanning calorimetry and X-ray powder diffraction. The system exhibits a significant solid solubility of the components, especially LiBr in the respective polymorphic modifications of CuBr. Another feature of the system CuBr–LiBr is the occurrence of five invariant three-phase equilibria, which have been assigned to one eutectic (684 K), one peritectoid (668 K), and three eutectoids (679, 645, and 521 K). From the experimental results, formation of a compound $LiCuBr_2$, at 521 K is discerned.

Keywords CuBr · DSC · LiBr · Phase diagram

Introduction

Studies of phase equilibria in the systems involving copper(I) halides are interesting, because chemical compounds with high electrical conductivity can be formed in these systems. High ionic conductivities of some solid phases found in the systems involving copper(I) halides and alkali-metal halides [1–13]. Several practical devices like solid state batteries, fuel cells, display panels, memory devices have been prepared and used [14]. In other hand, lithium is the lightest metal and has one of the highest standard reduction potentials with theoretical specific capacity of 3,860 Ah kg^{-1} in comparison with 820 Ah kg^{-1} for zinc and 260 Ah kg^{-1} for lead [15]. Since the standard reduction potential of lithium [16] is more negative than −3.0 V, the metal is thermodynamically unstable in protic solvents such as water, and the realization of practical lithium cells had to await the development of suitable non-aqueous electrolyte systems. It seems that it is a good idea to looking for new materials, stable at room temperature. However, polymorphism of the pure copper(I) halides [17–19] and their susceptibility to oxidation [20] are likely to make such investigations difficult. To our knowledge, no information on full phase diagram of the system copper(I) bromide–lithium bromide has been reported. Some preliminary results on phase equilibria were found in article [21]. Both components are difficult to operate, the former being sensitive to oxidation and the latter to traces of humidity. In this work, we present full results on phase diagram in the CuBr–LiBr system, based on experiments performed under vacuum or in an inert and exsiccated atmosphere.

E. Krzyżak (✉) · A. Wojakowska
Department of Inorganic Chemistry, Wrocław Medical University, ul. Szewska 38, 50-139 Wrocław, Poland
e-mail: edward.krzyzak@chnorg.am.wroc.pl

A. Wojakowski · M. Wołcyrz
Institute of Low Temperature and Structure Research, Polish Academy of Sciences, ul. Okólna 2, 50-422 Wrocław, Poland

Experimental

High purity CuBr and LiBr (Sigma Aldrich, 99.999%) were used, without further purification. Mixtures of salts were prepared by weighing appropriate quantities of CuBr and LiBr and put into flat, polished bottom ampoules, used afterwards for differential scanning calorimetry (DSC) measurements. Their outer diameter and height (after sealing) were 6 and 14 mm, respectively. All operations were prepared in a glove box containing argon (Labmaster 130 MBraun). Composition of mixtures was taken at intervals of 2–3 mol% or less. The accuracy of the composition determination was on the average 1 K and

Table 1 Temperature of phase transitions (DSC heating curves)

Sample	x_{CuBr}	x_{LiBr}	Temperature/K							
1	0.0000	1.0000	823							
2	0.0074	0.9926	822							
3	0.0115	0.9885	820							
4	0.0251	0.9749	817							
5	0.0311	0.9689	815							
6	0.0383	0.9617	814							
7	0.0434	0.9566	813							
8	0.0740	0.9260	807	683	679	667				
9	0.0900	0.9100	803	683	679	667				
10	0.1118	0.8882	797	682	679	668	520			
11	0.1307	0.8693	789	683	679	667	523			
12	0.1502	0.8498	783		679	668	519			
13	0.1650	0.8350	784	684	680	669	524			
14	0.1844	0.8156	774	684	680	668	522			
15	0.2035	0.7965	772	684	679	668	520			
16	0.2288	0.7712	767	683	679	668	523			
17	0.2386	0.7614	760	684	679	668	523			
18	0.2674	0.7326	751	684	680	669	526			
19	0.2909	0.7091	748		679	668	521			
20	0.3165	0.6835	741	687	679	668	522			
21	0.3528	0.6472	731	683	679	668	519			
22	0.3754	0.6246	721	684	680	669	519			
23	0.4391	0.5609	712	684	679	668	519			
24	0.4797	0.5203	699	684	679	668	520			
25	0.5039	0.4961		683	677	668	520			
26	0.5262	0.4738		684	680	669	519			
27	0.5618	0.4382		684	680	668	521			
28	0.5726	0.4274		686	680	669	519			
29	0.6161	0.3839	692	683			523		661	
30	0.6681	0.3319	696					687	659	528
31	0.7370	0.2630	708						653	593
32	0.7525	0.2475	710						649	619
33	0.7998	0.2002	713						647	624
34	0.8515	0.1485	718						644	634
35	0.8718	0.1282	730					722	645	
36	0.9053	0.0947	736					725	648	
37	0.9060	0.0940	735					726	646	
38	0.9284	0.0716	742					729	649	
39	0.9497	0.0503	746					731	651	
40	0.9618	0.0382	751					735	653	
41	0.9746	0.0254	752					736	654	
42	0.9876	0.0124	754					737	654	
43	1.0000	0.0000	759					740	657	

0.1 mol.%. The total weight of sample was 20–100 mg. The phases diagram was determined by DSC using Mettler Toledo DCS 25 measuring cell with TC15 Ta Controller. Samples for DSC measurements were heated beforehand under vacuum to a temperature 50 K above the corresponding melting point and then were homogenized at

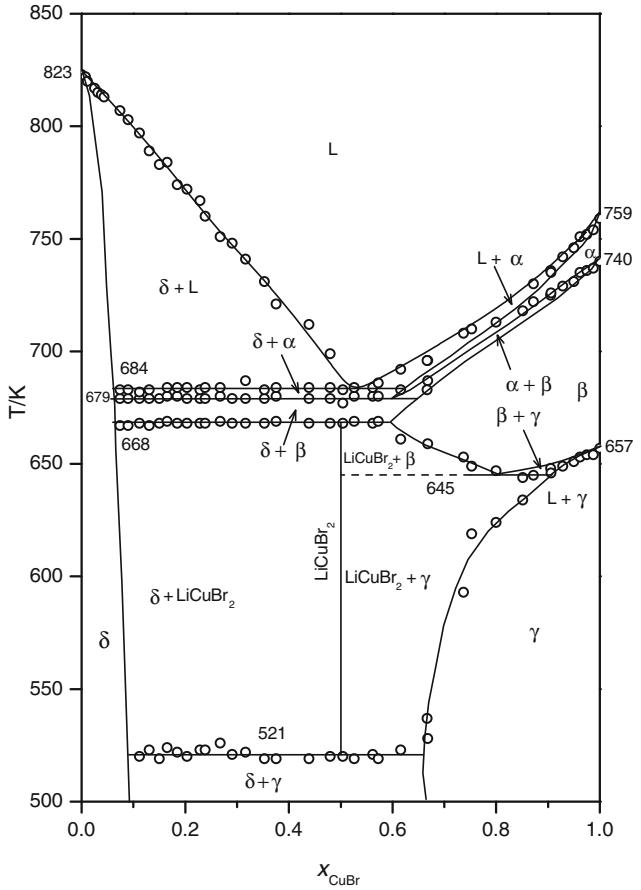

Fig. 1 Phase diagram of the CuBr–LiBr system

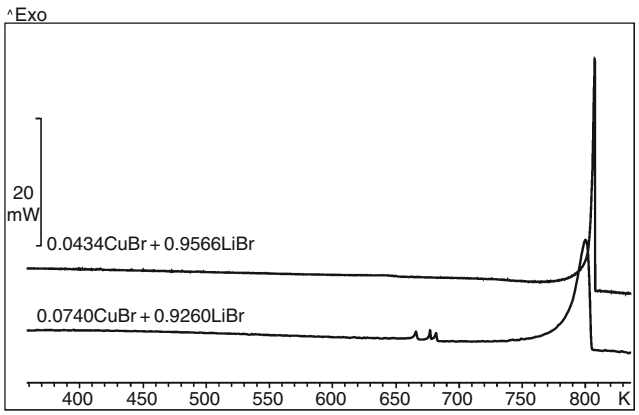

Fig. 2 DSC cooling curves for x(CuBr) = 0.0434 and x(CuBr) = 0.0740

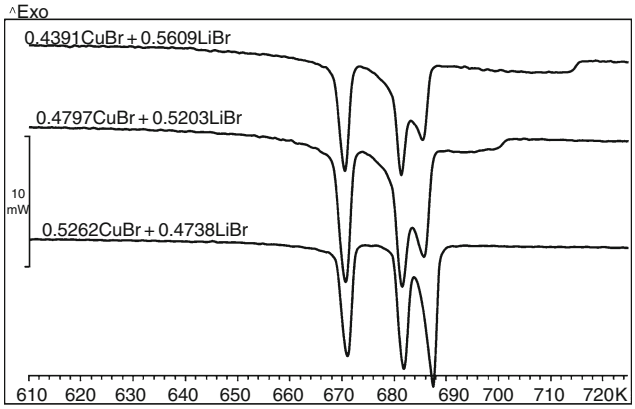

Fig. 3 DSC heating curves for x(CuBr) = 0.4391, 0.4797, and 0.5262

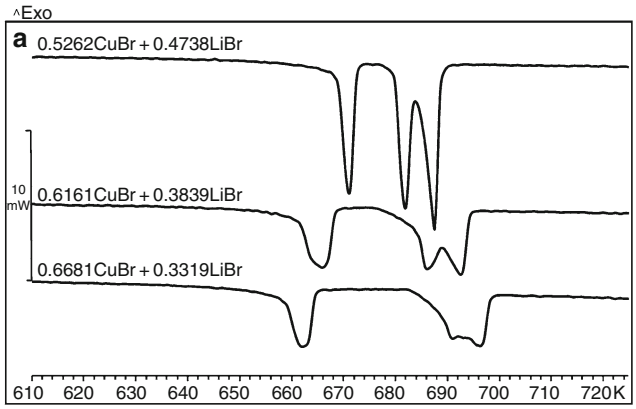

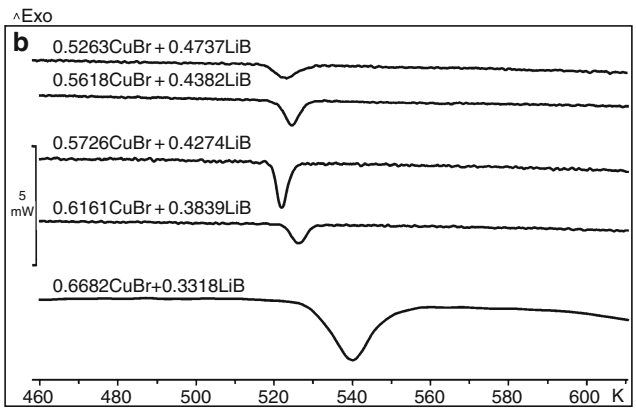

Fig. 4 **a** DSC heating curves for x(CuBr) = 0.5262, 0.6161, and 0.6681 in the higher temperature range. **b** DSC heating curves for x(CuBr) = 0.5262, 0.6161, and 0.6681 in the lower temperature range

about 400 K before experiment. All the homogenized CuBr + LiBr samples were first measured at the heating rate 1 K min^{-1} from about 300 K to melting and then cooled back with the same rate. Besides the above runs, other heating and cooling rates: (0.5, 5, 7.5, 10 K min^{-1}) were also used when needed. For the X-ray diffraction experiments, a STOE powder diffraction system was used (Cu$K\alpha$ radiation, $10° \leq 2\theta \leq 90°$, step scan mode with a step size of 0.02° and counting time of 15 s per data point). Mixtures were prepared in a glove box containing argon and then sealed under vacuum, heated to melting and homogenized. After homogenization, samples were loaded

into glass capillaries of 1 mm diameter and 30 mm length, in the glove box. The composition of 0, 5, 7.5, 20, 33, 50, 77, 80, 88, 100 mol.% CuBr were taken. X-ray powder diffraction patterns were obtained at room temperature.

Results and discussion

The results of the DSC experiments of all samples are summarized in Table 1. DSC curves for cooling runs showed appreciable supercooling effects and hence only the heating curves were analyzed to gather data. The accuracy of the temperature and the composition determination was on the average 1 K.

The phase equilibrium diagram of the CuBr–LiBr system determined in this study is presented in Fig. 1. Examples of DSC heating and cooling curves, which have been essential for the construction of the phase diagram of the CuBr–LiBr system, are given in Fig. 2, 3, 4, 5, 6. X-ray diffraction patterns are presented in Fig. 7a, b.

The DSC curves obtained for pure components show endothermic peaks corresponding to the melting of the pure phases and two peaks corresponding to the phase transition for pure CuBr. For the samples of compositions less than $x(\mathrm{CuBr}) < 0.0740$, only one peak was observed. For the mixture with higher concentration CuBr, DSC curves show more endothermic peaks (Fig. 2). It seems that the solid solution of CuBr in LiBr (δ) does not exceed $x(\mathrm{CuBr}) = 0.077$ at room temperature. It shows a little increase in the range of composition with decreasing temperature. The X-ray diffraction analysis of the samples $x(\mathrm{CuBr}) < 0.008$ at room temperature after homogenization, showed the presence of only LiBr (Fig. 7a). Similar solid solution was reported for the CuCl–LiCl system [22].

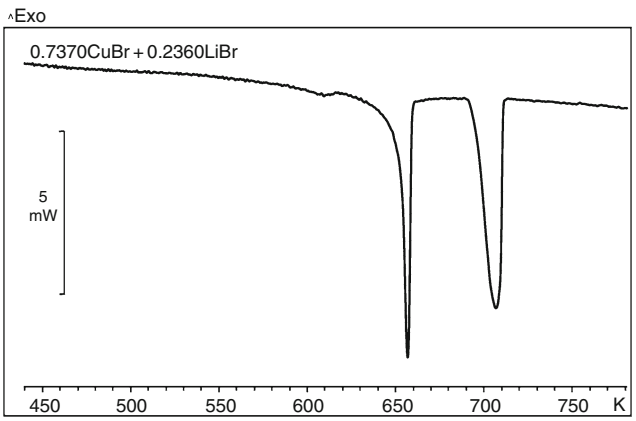

Fig. 5 DSC heating curves for $x(\mathrm{CuBr}) = 0.7370$

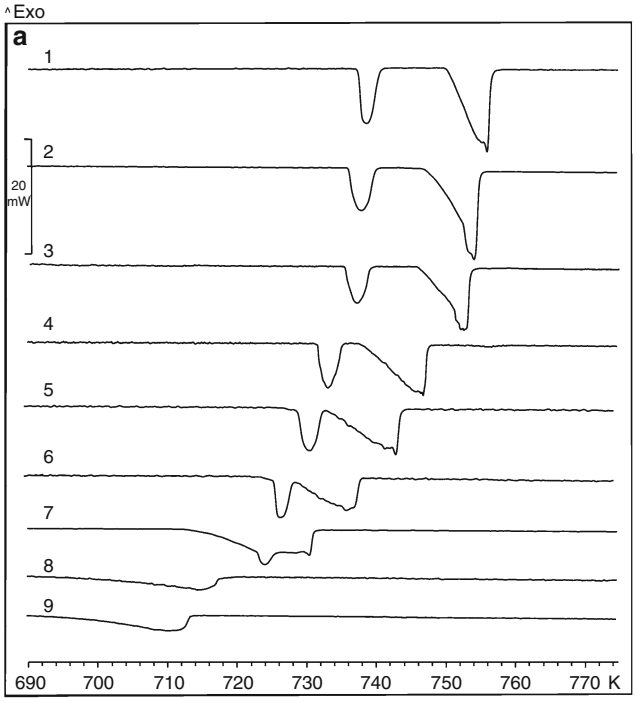

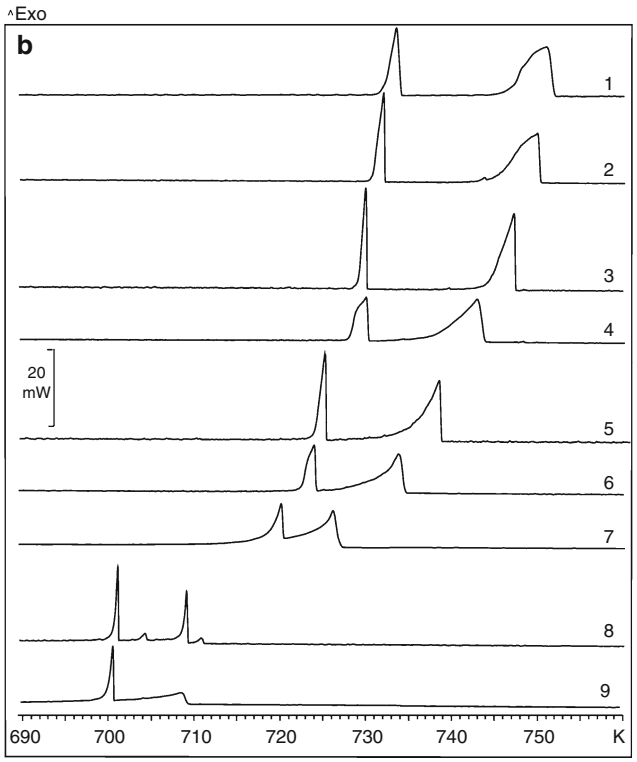

Fig. 6 **a** DSC heating curves for $x(\mathrm{CuBr}) = 0.9876$ (*1*), 0.9746 (*2*), 0.9618 (*3*), 0.9494 (*4*), 0.9284 (*5*), 0.9053 (*6*), 0.8718 (*7*), 0.8515 (*8*), 0.7998 (*9*). **b** DSC cooling curves for $x(\mathrm{CuBr}) = 0.9876$ (*1*), 0.9746 (*2*), 0.9618 (*3*), 0.9494 (*4*), 0.9284 (*5*), 0.9053 (*6*), 0.8718 (*7*), 0.8515 (*8*), 0.7998 (*9*)

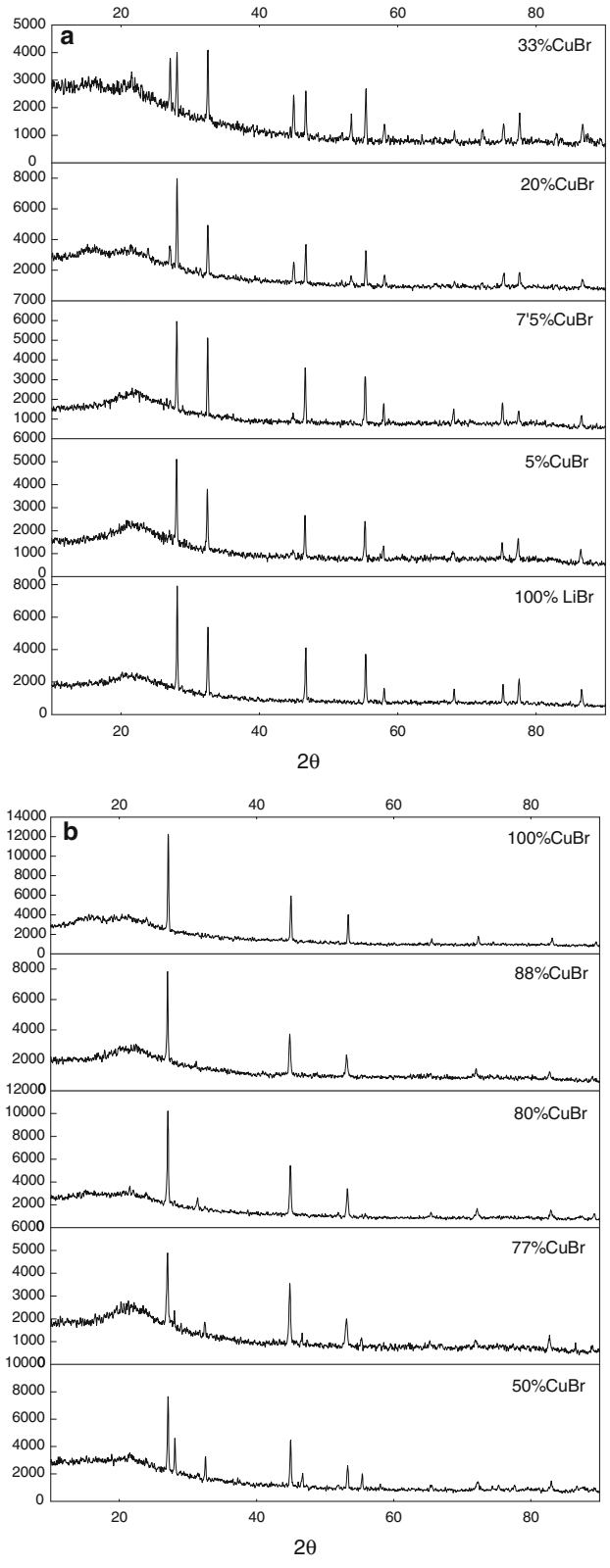

Fig. 7 **a** X-ray powder diffraction patterns of pure components (γ-CuBr, LiBr) and their mixtures quenched to room temperature. **b** X-ray powder diffraction patterns of pure components (γ-CuBr, LiBr)and their mixtures quenched to room temperature

In the system CuBr–LiBr, there are five invariant three-phase equilibria, which have been assigned to one eutectic (684 K), one peritectoid (668 K), and three eutectoids (679, 645, and 521 K). DSC curves obtained for samples of composition $x(\mathrm{CuBr}) = 0.4391$, 0.4797, 0.5262, at the range temperature 610–720 K are shown in Fig. 3. Three endothermic peaks are observed. The thermal effect with a highest temperature (684 K) represents an eutectic reaction. The Tamman method [23] shows that the maximum value of the thermal effect at 684 K (for all samples with this peak) is given for the mixture with concentration CuBr about $x = 0.53$. The eutectic thermal effect goes to zero for compositions corresponding to $x(\mathrm{CuBr}) = 0.06$. This may indicate some solid solubility.

Apart from the eutectic reaction at 684 K, clearly marked invariances at 668 K and 521 K were found and interpreted as solid-state reactions resulting in the formation and decomposition of a new phase, stable only between 521 and 668 K. X-ray diffraction experiments also show that this intermediate phase cannot be quenched to room temperature (Fig. 7a, b). The maximal thermal effect of both reactions occurred at the same composition, about $x(\mathrm{CuBr}) = 0.50$ (Fig. 8), indicating the formula $LiCuBr_2$. However, a variable composition of the compound, stretching to the CuBr side, cannot be excluded since thermal events corresponding to the eutectoid reaction at 645 K are not shown by DSC curves between $x(\mathrm{CuBr}) = 0.50$ and $x(\mathrm{CuBr}) = 0.75$. This is rather unexpected since 1:1 compounds rarely appear in the copper(I) halide–alkali halide systems [24].

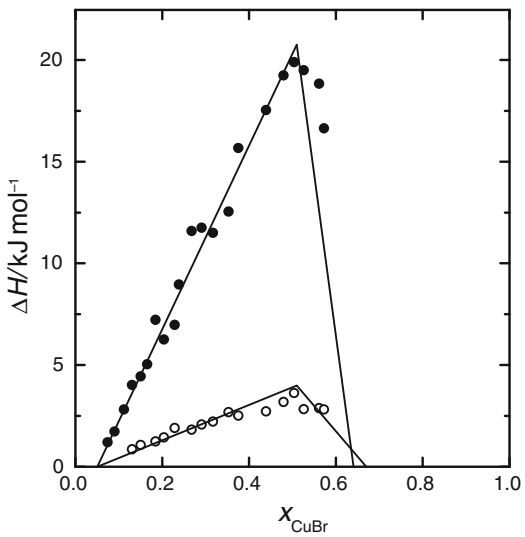

Fig. 8 Tamman triangles for solid state reactions at 521 K (*open circle*) and 668 K (*closed circle*), respectively, in the CuBr–LiBr system

Differential scanning calorimetry heating curves for x(CuBr) = 0.5262, 0.6161, and 0.6681 are shown in Fig. 4a, b. It seems that thermal effect at temperature 512 K is not observed for the sample with concentration x(CuBr) = 0.6681. The temperature of a peak is about 10 K higher and the value of effect is higher than for samples with lower concentration CuBr. The X-ray diffraction analysis of the sample x(CuBr) = 0.80 at room temperature, after homogenization, showed the presence of only CuBr and for sample x(CuBr) = 0.77 showed the presence of CuBr and LiBr (Fig. 7b). The solid solubility of LiBr in γ-CuBr is formed with a limit at room temperature about x(CuBr) = 0.78 and it increases to maximum value about x(CuBr) = 0.67 in temperature 521 K. Figure 5 shows a DSC curve obtained for sample with concentration x(CuBr) = 0.7370. The first small thermal effect is appeared at temperature about 600 K (equilibrium γ-CuBr with two phases $LiCuBr_2$ + γ-CuBr). The next one, there is in temperature about 650 K. It was indicated as a γ-CuBr = β-CuBr transition. The last peak (temperature 708 K) consists more then one thermal effect, probably, with small difference of temperature. The DSC traces obtained for composition between x(CuBr) = 0.7998 and x(CuBr) = 0.9876, in the high-temperature range (Fig. 6a, b) shown 3–4 near thermal effects. Hence, at the eutectic temperature of 684 K, the liquid mixture is in equilibrium with two solid solutions: CuBr in LiBr and the solid solution of LiBr in α-CuBr. The latter decomposes eutectoidally at 679 K into the solid solution CuBr in LiBr and the solid solution of LiBr in β-CuBr. The limits of the solid solubility of LiBr in α-CuBr and β-CuBr were estimated to be x(CuBr) = 0.60 and x(CuBr) = 0.65, and a range for the temperature for the existence of high-temperature α and β superionic phases was found to stretch to 679 and 645 K, respectively, i.e., 60 and 95 K below the α/β phase transition in pure CuBr. Similar wide solid solutions based on CuBr modifications were reported for the CuBr–AgBr system [25]. The extended solid solutions formed in the CuBr–LiBr system are no surprise since the effective radii of Cu^+ and Li^+ were often considered as being close to each other, both having a value of about 0.5 Å [26, 27].

Conclusions

The phase diagram for CuBr–LiBr system is constructed based on DSC studies and XRD data on samples of various compositions of CuBr and LiBr. Due to susceptibility to oxidation of CuBr and high hygroscopicity of LiBr sample preparation and experiment required special conditions. The comprehensive studies have shown that there are not stable compounds at room temperature. From the experimental results, formation of a compound $LiCuBr_2$, at 521 K is discerned. This is rather unexpected since 1:1 compounds rarely appear in the copper(I) halide–alkali halide systems [24]. The system exhibits solid solution at both the terminal compositions, especially LiBr in the respective polymorphic modifications of CuBr. Due to polymorphism of the pure CuBr, the phase diagram is complicated. Five invariant three-phase equilibria have been determined: one eutectic (684 K), one peritectoid (668 K), and three eutectoids (679, 645, and 521 K).

References

1. Bradley JN, Greene PD. Solids with high ionic conductivity in group 1 halide systems. Trans Faraday Soc. 1967;63:424–30.
2. Matsui T, Wagner JB Jr. High conductivity cuprous halide–metal halide systems. J Electrochem Soc. 1977;124:937–40.
3. Matsui T, Wagner JB Jr. Investigations on a high conductivity solid electrolyte system, RbCl plus CuCl. J Electrochem Soc. 1977;124:941–4.
4. Kanno R, Takeda Y, Masuyama Y, Yamamoto O, Takahashi T. Phase diagram and high copper ion conductivity of the copper(I) chloride-rubidium chloride system. Solid State Ion. 1983;11(3):221–6.
5. Gaines JM, Geller SJ. Electrical conductivity and crystal structure of the solid electrolyte Rb//4Cu//9Cl//1//3. Electrochem Soc. 1986;133:1501–7.
6. Gaines JM, Geller S. Anisotropic electrical conductivity of the solid electrolyte $Rb_4Cu_9C_{113}$. Phys Rev B. 1986;34:8963–6.
7. Warner TE, Fray DJ. A study of phase stability in the rubidium–copper(I)-chloride system. J Solid State Chem. 1989;83:366–9.
8. Bazan JC, Pettigrosso RS, Garcia NJ, Dristas JA. On the influence of Cs(I)-doping on the electrical conductivity of cuprous bromine. Solid State Ion. 1996;86–88:241–5.
9. Schmidt JA, Lescano GM, Prat MR, Dristas JA. Influence of $CsCu_2C_{13}$ on the electrical conductivity of CuCl. Solid State Ion. 1998;112:63–7.
10. Hull S, Keen DA, Sivia DS, Berastegui PJ. Crystal structures and ionic conductivities of ternary derivatives of the silver and copper monohalides: I. Superionic phases of Stoichiometry MA_4I_5: $RbAg_4I_5$, KAg_4I_5, and KCu_4I_5. Solid State Chem. 2003;165:363–71.
11. Keen DA, Hull S, Barnes AC, Berastegui P, Crichton WA, Madden PA, Tucker MG, Wilson M. Nature of the superionic transition in Ag+ and Cu+ halides. Phys Rev B. 2003;68:141171–1411711.
12. Hull S, Berastegui PJ. Crystal structures and ionic conductivities of ternary derivatives of the silver and copper monohalides - II: Ordered phases within the $(AgX)_x$–$(MX)_{1-x}$ and $(CuX)_x$-$(MX)_{1-x}$ (M = K, Rb and Cs; X = Cl, Br and I) systems. Solid State Chem. 2004;177:3156–73.
13. Arai M, Sakuma T, Atake T, Kawaji H. Phase transition of CuITe. J Therm Anal Calorim. 2002;69:905–8.
14. Viswanath AK, Radhakrishna S. Copper ion conductors. In: Takahashi T, editor. High conductivity solid ionic conductors—recent trends and applications. New York: World Scientific Publishing Company; 1989. p. 280–326.
15. Vincent CA. Lithium batteries: a 50-year perspective, 1959–2009. Solid State Ion. 2000;134:159–67.
16. Fischer L, Winkler G, Jander G. Recent findings concerning the electrochemistry of non-aqueous solutions. Z Elektrochem. 1958;62:1–8.

17. Lorenz MR, Prener JS. Preliminary study of a high-temperature phase in cuprous chloride. Acta Crystallogr. 1956;9:538–9.
18. Bűhrer W, Hälg W. Crystal structure of high-temperature cuprous iodide and cuprous bromide. Electrochim Acta. 1977;22:701–4.
19. Schwab C, Goltzene A. Cuprous halides. Prog Cryst Growth Charact. 1982;5:233–76.
20. Cotton F, Wilkinson G, Murillo C, Bochman M. Advanced inorganic chemistry. 6th ed. New York: Wiley; 1999. p. 855.
21. Wojakowska A, Krzyżak E, Wojakowski A, Wołcyrz MZ. Phase equilibria in copper(I) bromide–MBr systems (M = Li, Na, K). Naturforsch. 2007;62a:507–12.
22. Korreng E. Kristallographische und therniische Untersuchung von binaren Sjstemen aus Thallochlorid und Chloriden zweiwertiger Metalle. Neues Jahrb Mineral Geolog. 1914;37:51–124.
23. Tamman G. Über die Anwendung der thermischer Analyse III. Z Anorg Chem. 1905;47:289–313.
24. Wojakowska A, Krzyżak E. Factors affecting the general shape of the phase diagram and compound formation in the binary copper(I) halide–alkali-metal halide systems. J Therm Anal Calorim. 2006;83:597–601.
25. Saito M, Takahashi H, Tamaki S. Phase diagram and thermodynamic properties of $(Ag_xCu_{1-x})Br$. Solid State Ion. 1989;35:359–65.
26. Shannon RD, Prewitt CT. Effective ionic radii in oxides and fluorides. Acta Crystallogr. 1969;B25:925–46.
27. Dantzer P. Thermodynamics of mixing of binary liquid mixtures. Copper(I) halides–alkali halides. J Phys Chem. 1981;85:724–7.